

Autoregressive Image Generation Guided by Chains of Thought

Miaomiao Cai^{1*} Guanjie Wang^{1*} Wei Li^{2†} Zhijun Tu² Hanting Chen² Shaohui Lin³ Jie Hu^{2†}

¹University of Science and Technology of China

²Huawei Noah's Ark Lab

³East China Normal University

mmcai@mail.ustc.edu.cn, wei.lee@huawei.com, hujie23@huawei.com

Abstract

In the field of autoregressive (AR) image generation, models based on the ‘next-token prediction’ paradigm of LLMs have shown comparable performance to diffusion models by reducing inductive biases. However, directly applying LLMs to complex image generation can struggle with reconstructing the structure and details of the image, impacting the accuracy and stability of generation. Additionally, the ‘next-token prediction’ paradigm in the AR model does not align with the contextual scanning and logical reasoning processes involved in human visual perception, limiting effective image generation. Chain-of-Thought (CoT), as a key reasoning capability of LLMs, utilizes reasoning prompts to guide the model, improving reasoning performance on complex natural language process (NLP) tasks, enhancing accuracy and stability of generation, and helping the model maintain contextual coherence and logical consistency, similar to human reasoning. Inspired by CoT from the field of NLP, we propose autoregressive Image Generation with Thoughtful Reasoning (IGTR) to enhance autoregressive image generation. IGTR adds reasoning prompts without modifying the model structure or raster generation order. Specifically, we design specialized image-related reasoning prompts for AR image generation to simulate the human reasoning process, which enhances contextual reasoning by allowing the model to first perceive overall distribution information before generating the image, and improve generation stability by increasing the inference steps. Compared to the AR method without prompts, our method shows outstanding performance and achieves an approximate improvement of 20%.

1. Introduction

Large language models (LLMs) have a significant impact on the field of artificial intelligence, changing approaches

¹Equal Contribution

²Corresponding author

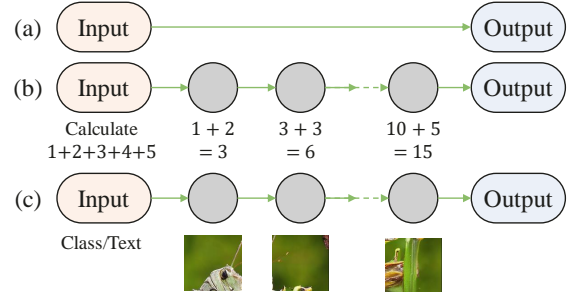


Figure 1. Illustration of the reasoning process based on LLMs. The grey circles represent reasoning prompts. (a) General AR model reasoning process. (b) CoT utilizes intermediate textual reasoning prompts to perform text reasoning tasks. (c) Image Generation with Thoughtful Reasoning (IGTR) incorporates image-related reasoning prompts to perform image generation tasks.

to addressing traditional challenges in natural language processing and machine learning [1, 36]. Recently, in the field of image generation, there has been widespread attention on autoregressive (AR) image generation based on the LLMs. For example, LlamaGen [35] employs the AR model based on the ‘next-token prediction’ paradigm of large language models for image generation, which reduces the inductive biases on visual signals. Under this design, LlamaGen has demonstrated comparable results to popular diffusion-based image generation models [24, 27], which shows that the AR model can serve as the foundation for advanced image generation systems.

However, directly applying LLMs to the image generation task, which is much more complex than the text generation task, could result in the model struggling to reconstruct the structure and details of the image, thus affecting the accuracy of the generated results and the stability of the generation process. Additionally, when humans perceive complex visual information, they typically scan the entire image before focusing on the target. In contrast, the ‘next-token prediction’ paradigm in AR image generation does not align with the contextual sequence and logical reason-

ing required for real image generation.

In the field of natural language processing (NLP), one of the most distinguishing abilities of LLMs is the exceptional reasoning capabilities, with Chain-of-Thought prompting (CoT) [39] serving as a key technique. Compared to the general AR model reasoning process in Fig. 1 (a), CoT (Fig. 1 (b)) leverages intermediate reasoning prompts to guide the model, achieving significant performance improvements in complex tasks such as arithmetic, common-sense reasoning, and symbolic inference. This structured reasoning approach enhances the stability of the reasoning process and reduces errors caused by the complexity of the task. Moreover, CoT enables the model to reason and solve problems more like humans by incorporating intermediate reasoning prompts, allowing the model to maintain contextual coherence and logical consistency throughout the reasoning process.

Despite differing in task formulation from the logical reasoning tasks commonly encountered in NLP-based LLMs, AR image generation can be attributed to a similar organized structure, where each subtask is solved based on the state of the previous one. As a result, autoregressive image generation also has the powerful reasoning capabilities of LLMs. Therefore, inspired by CoT from the field of NLP, to enhance the ability of LLMs to handle complex image generation tasks, we propose autoregressive Image Generation with Thoughtful Reasoning (IGTR) based on the AR model by adding intermediate reasoning prompts for image generation, without modifying any model structure or the autoregressive raster generation order, which is shown in Fig. 1 (c). Our method improves both the accuracy and stability of the generation and strengthens the logical generation capabilities of the images. Specifically, we design specialized image-related reasoning prompts for AR image generation as the intermediate reasoning process, simulating the human reasoning process by allowing the model to first perceive overall distribution information (such as the universal distribution of the image dataset or the overall distribution information of a specific category) before generating the image. The reasoning prompt enhances contextual reasoning of generation, and also improves stability during the generation process by increasing the inference step.

Our contributions are as follows:

1. We propose autoregressive Image Generation with Thoughtful Reasoning (IGTR), where we introduce CoT technology to autoregressive image generation by incorporating intermediate reasoning prompts for image generation. IGTR enhances the capability of large language models in the complex image generation task, without modifying any model structure or the autoregressive raster generation order.
2. We design specialized image-related reasoning prompts for AR image generation as the intermediate reasoning

process, allowing the model to first perceive overall distribution information before generating the image, which enhances contextual reasoning of generation, and also improves stability during the generation process by increasing the inference step.

3. Compared to the AR method without prompts, our method shows outstanding performance and achieves an approximate improvement of 20%.

2. Related Work

2.1. Chain-of-Thought

Large language models (LLMs) exhibit impressive reasoning capabilities due to advanced language generation abilities. Chain-of-Thought (CoT), as a key technique, is specifically designed for multi-step reasoning [39]. Traditional prompting methods [3] have shown limited effectiveness on complex tasks that require reasoning capabilities. Inspired by the concept of using intermediate steps to address reasoning problems [5, 20], CoT simulates the human process of reasoning and problem-solving by incorporating intermediate reasoning prompts, allowing the model to maintain contextual coherence and logical consistency during the reasoning process [39]. CoT has been shown to significantly enhance the performance of LLMs on complex tasks, while also improving the stability of the reasoning process [39].

Chain-of-Thought has been applied to many different tasks, including natural language processing [21, 38, 40, 41] and multi-modal large language models [22, 23, 45]. To the best of our knowledge, in the field of AR image generation, the capabilities of CoT have not yet been explored, which can provide the intermediate reasoning process for complex image generation tasks, to enhance image generation capabilities, strengthen the logical generation of images, and improve the stability of generation.

2.2. Autoregressive Visual Generation Methods

Visual generation has received significant attention in recent years, especially with the development of deep learning architectures and generative models. One key trend is the use of autoregressive models, which show significant generality and potential due to their strong connection with NLP. However, there is no mature or well-established community, and further efforts are needed to overcome challenges and fully realize their capabilities. Existing autoregressive generation methods are commonly divided into two approaches: BERT-style mask autoregressive models and GPT-style autoregressive models. Mask Autoregressive methods [4, 18, 19, 43], inspired by BERT-style pre-training [15], generate images by predicting the random masked tokens. Instead, another kind of autoregressive method [8, 26, 42], inspired by GPT [25], predicts the next token in a sequence, which

applies the image tokenization [16, 37] to transform images to discrete space. Recently, based on autoregressive methods, LlamaGen [35] adapts large language model architectures like Llama [36], to autoregressively predict image tokens by applying the ‘next-token prediction’ paradigm to visual generation, which achieve decent performance in image generation.

2.3. Other Visual Generation Methods

In addition to AR visual generation methods, significant efforts have also been made in exploring other forms of visual generation models. Generative Adversarial Networks (GANs) is the earliest approaches, leveraging adversarial training to generate images [2, 10, 13, 14, 30]. Diffusion models, an alternative approach, generates images by gradually refining random noise through a series of learned steps [6, 12, 24, 27, 32, 33]. GANs-based and diffusion-based methods show promising performance because their community are relatively complete. If AR models are to surpass them, further iterations and development of AR models are needed.

3. Method

3.1. Preliminary

AutoRegressive Modeling (AR). First, an image I in the form of $H \times W \times 3$ is quantized into discrete tokens map X in the form of $h \times w$ by an image tokenizer with $h = H/p, w = W/p$, where p is the down-sampling rate of the tokenizer. Then, according to the raster scanning order, X reshape into 1d sequence $(x_1, x_2, \dots, x_t), t = h * w$ and the approximate maximum log-likelihood estimation 1 is used as the training target of the model θ .

$$\theta_{target} = \arg \max_{\theta} \sum_{t=1}^T P_{\theta}(x_t | x_{<t}) \quad (1)$$

In the image generation process, the AR predicts the image token (x_1, x_2, \dots, x_t) according to the condition c in a prediction manner of ‘next-token prediction’ $\prod_{t=1}^T P(x_t | x_{<t}, c)$, and finally converts the image token into an image by using a decoder of the image tokenizer.

3.2. Ours

3.2.1 Overview

Our method still adapts the image tokenizer architecture and ‘next-token prediction’ prediction form of the classic AR model. On this basis, we introduce a set of reasoning prompt $\tilde{S} = (s_1, s_2, \dots, s_k)$ in the training and inference process, just like the CoT technique in the language model, and modify the model θ training target to maximize the log-likelihood function 2. The way model inference is change

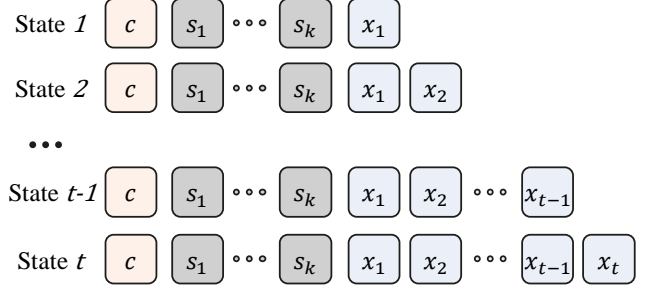


Figure 2. The exhibition of different state with k-length reasoning prompt.

to $\prod_{t=1}^T P(x_t | x_{<t}, \tilde{S}, c)$.

$$\sum_{t=1}^N \log P_{\theta}(x_t | x_{<t}, \tilde{S}, c) \quad (2)$$

3.2.2 Theoretical Analysis

The introduced reasoning prompt is $\tilde{S} = (s_1, s_2, \dots, s_k)$, the generated token sequence is $\tilde{X} = (x_1, x_2, \dots, x_t)$, the condition is c , and the model parameter is θ .

Training Stage We refer to the derivation of CoT techniques for LLMs in the context of general dynamic programming problems by Feng *et al.* [9], and analyse the impact of introducing CoT in our model while training. As shown in Figure 2, one sequence shows the different state i with unidirectional transitions between states constrained by the time step i . Since there is a target sequence present, for each token prediction during model training, there exists an optimal solution token (*i.e.*, the target token at the corresponding position). Thus, we can express the state transition function as follows:

$$T(i, j) = \begin{cases} p_j & \text{if } i = j - 1 \\ p_j * T(i, j - 1) & \text{if } i < j - 1 \end{cases} \quad (3)$$

p_j represents the probability of the model predicting the optimal state j token at time step j . $T(i, j)$ denotes the probability of transitioning from the optimal state i to the optimal state j , where the optimal state is defined as a state in which all tokens are the optimal tokens for current position. Thus, we can formulate $T_{AR}(1, t)$ for the classic AR model and $T_{IGTR}(1, t)$ for our method as follows:

$$T_{AR}(1, t) = T(1, 2) * T(2, t) \quad (4)$$

$$T_{IGTR}(1, t) = T(1, 2) * T(2, k + 1) * T(k + 1, t) \quad (5)$$

where k represents the length of the sequence \tilde{S} .

It is easy to infer that, under the ideal condition with the same target, both $T_{AR}(1, t)$ and $T_{IGTR}(1, t)$ should equal

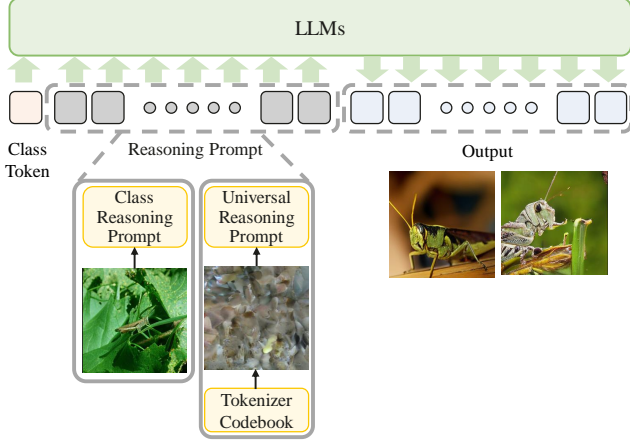


Figure 3. Our method first receives *Class Token* and *Reasoning Prompt* as input, and then follows the ‘next-token prediction’ to generate images.

to the expression $\prod_{t=1}^T P(x_t|x_{<t}, c)$, which corresponds to the maximum likelihood estimation (*MLE*) of the target generated image. However, since the limitation of the model ability, what we can do is to approximate the target distribution through *MLE*, these tree equations $T_{AR}(1, t)$, $T_{IGTR}(1, t)$ and $\prod_{t=1}^T P(x_t|x_{<t}, c)$ are not exactly equal. In this case, due to the introduction of reasoning prompt, our method, compared to the classic AR method, gains an additional term $T(2, k+1)$, which allows the model have a set of weights that can be dynamically adjusted based on the condition c . Therefore, compared to $T_{AR}(1, t)$, $T(2, k+1)$ makes $T_{IGTR}(1, t)$ more easily approximated to the target distribution, enabling a model with the same parameter count to converge faster when trained on the same amount of data.

The final loss of the model is constrained by the cross-entropy between the target sequence and the generated sequence \tilde{X} .

Inference Stage We analyse the impact of introducing reasoning prompt on the model’s inference phase from the perspective of information entropy. The information entropy of the classic AR model during inference can be expressed as $H(\tilde{X}|c)$, while the information entropy of our method with reasoning prompt during inference can be expressed as $H(\tilde{X}|\tilde{S}, c)$. With the definition of entropy, we can derive Eq 6 as follows:

$$H(\tilde{X}|\tilde{S}, c) = H(\tilde{X}, \tilde{S}|c) - H(\tilde{S}|c) \quad (6)$$

Then we can derive the inequality in eq 7.

$$\begin{aligned} H(\tilde{X}|\tilde{S}, c) - H(\tilde{X}|c) &= \\ H(\tilde{X}, \tilde{S}|c) - H(\tilde{X}|c) - H(\tilde{S}|c) &\leq 0 \end{aligned} \quad (7)$$

Model	Parameters	Layers	Hidden Size	Heads
Ours-B	111M	12	768	12
Ours-L	343M	24	1024	16
Ours-XL	775M	36	1280	20
Ours-XXL	1.4B	48	1536	24

Table 1. Model sizes and architecture configuration of our method.

This inequality suggests that, by incorporating reasoning prompt, compared to classic AR model, our method has less uncertainty during inference, which means the generation process is more stable. This reduction in uncertainty helps effectively minimize inconsistencies in the image details represented by the tokens, leading to higher-quality generated images. The more stable token generation process ensures that the generated sequence better preserves the coherence of the visual structure, resulting in images with fewer artifacts and better alignment with the target distribution.

3.2.3 Reasoning Prompt

As shown in Figure 3, we choose two different type of reasoning prompt \tilde{S} to incorporate into the model’s training and inference process.

1. We randomly select an image that is different from the training target while it’s still under the same class with the training target. After passing it through the image tokenizer, it is converted into tokens, which are then concatenated with the condition c and input into the model. During inference, we randomly choose an image, tokenize it, and use the resulting tokens as input directly.
2. We sample a set of indices from the codebook of the image tokenizer based on a uniform distribution, selecting each index with equal probability. The sampled set of indices is then concatenated with the condition c and used as the input to the model.

These two different reasoning prompts represent two distinct distributions used to guide the model in generating images. The first prompt corresponds to a specific category distribution called *Class Reasoning Prompt*, aimed at helping the model better understand the distribution corresponding to the given condition, thereby generating images that more clearly represent the category information. The second prompt represents a more universal image distribution called *Universal Reasoning Prompt*, designed to encourage the model to generate more diverse and varied images.

4. Experiment

In this section, we describe the implementation details of our approach in Sec. 3.2.3. We then provide ablation studies on important design decisions in Sec. 4.2. Following

Training	Inference	FID↓	IS↑	Precision↑	Recall↑
Non Reasoning Prompt		5.46	193.61	0.83	0.45
Class Reasoning Prompt	Class Reasoning Prompt	4.34	226.31	0.84	0.46
	Universal Reasoning Prompt	4.36	227.44	0.84	0.46
Universal Reasoning Prompt	Class Reasoning Prompt	4.42	217.66	0.85	0.45
	Universal Reasoning Prompt	4.39	222.80	0.85	0.46
Mixture		4.55	235.13	0.86	0.44

Table 2. Ablation study for different types of reasoning prompts using for training or inference. ‘↓’ or ‘↑’ indicate lower or higher values are better. ‘Mixture’ means we combine two different prompts for training and inference,

that, the main results and the visualizations are discussed in Sec. 4.3.

4.1. Experiment Setting

Model Architecture Following prior work which use a VQ tokenizer to tokenize the input images into discrete tokens, we use the VQGAN reported in LlamaGen [35] with the official weight trained on ImageNet. Our model architecture is largely based on Llama [36], applying pre-normalization using RMSNorm [44], SwiGLU [31] activation function, and 2D rotary positional embeddings [34] at each layer of our model. We use model of different configuration including B (111M), L (343M), XL (775M), and XXL (1.4B). The detailed architecture configuration and size are shown in Table 1.

Training Setup We experiment on ImageNet [28] at a resolution of 256×256 based on the class to image task. To accelerate training, we pre-tokenize the entire training dataset before training using the VQGAN tokenizer reported in LlamaGen [35]. Additionally, we improve the diversity of the pre-tokenized dataset by applying the ten-crop transformation [35]. Following the classic evaluation suite provided by [7], we evaluate FID [11] as the main metric and also report IS [29], Precision, and Recall as references metrics. Unless otherwise specified, models are trained for 300 epochs and the default inference setting is top-k=0, top-p=1.0, temperature=1.0, number of reasoning prompt=256. Additionally, the dropout for the class condition embedding in Classifier-Free Guidance (CFG) is set to 1.75 by default. All models are trained using the base learning rate of 0.0001 and the batch size of 256. AdamW optimizer is set with $\beta_1 = 0.9$ and $\beta_2 = 0.95$, weight decay is set to 0.05, and gradient clipping is set at 1.0. A dropout rate of 0.1 is applied to the input token embeddings, attention modules, and the FFN module.

4.2. Ablation Study

This section mainly includes the properties of our method, as well as the choice of parameters.

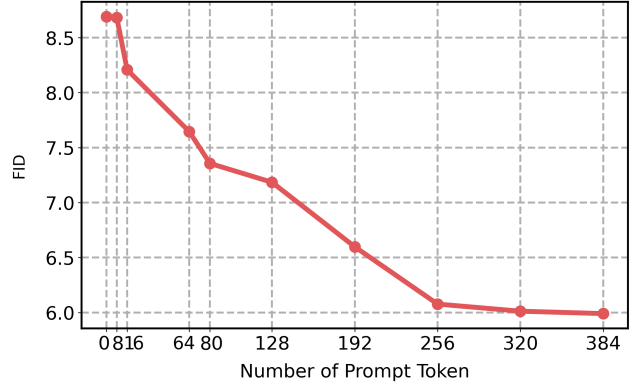


Figure 4. Ablation study for different numbers of prompt tokens.

4.2.1 Robustness of IGTR

To evaluate the robustness of proposed IGTR, we conduct experiments using different types of reasoning prompts. Specifically, we use two types of prompts mentioned in Sec. 3.2.3: class reasoning prompt and universal reasoning prompt, as the intermediate reasoning process for our image generation. We evaluate the effectiveness and robustness of IGTR by comparing the results with consistent reasoning prompts (*i.e.*, the same reasoning prompt used during both training and inference) and inconsistent reasoning prompts (*i.e.*, different reasoning prompts used during training and inference). In addition, we also combine two different prompts for training and inference, with each having a 50% probability of being selected. We train the model with 111M parameters for 300 epochs, which is the same settings as those in LlamaGen [35]. The baseline is LlamaGen [35], an AR image generation model based on the Llama architecture without our reasoning prompt.

The results are shown in Table 2, with the following observations: (1) Regardless of whether we use consistent or inconsistent reasoning prompts for training and inference, and regardless of which reasoning prompt we choose for the intermediate reasoning process, our method consistently outperforms baseline without reasoning prompt, achieving an approximate 20% improvement in FID scores. This

Inference	FID↓	IS↑	Precision↑	Recall↑
Non Reasoning Prompt	8.69	124.44	0.79	0.47
Reasoning After Generation	8.70	122.79	0.79	0.47
Blank Prompt	8.65	123.15	0.80	0.43
IGTR	6.07	174.48	0.82	0.44

Table 3. Ablation study for different variations of prompting. ‘↓’ or ‘↑’ indicate lower or higher values are better.

CFG	FID↓	IS↑	Precision↑	Recall↑
1.25	7.14	106.97	0.71	0.58
1.50	5.47	167.61	0.80	0.52
1.75	4.39	222.80	0.85	0.46
2.00	5.24	266.85	0.88	0.40
2.25	6.83	304.32	0.91	0.36
2.50	8.49	329.75	0.92	0.31

Table 4. Ablation study for different CFG settings.

demonstrates that our method exhibits good robustness. (2) The performance of the class reasoning prompt is better than that of the universal reasoning prompt. This is because focusing on the overall distribution of a specific class is more informative than considering the overall distribution of the entire image set, as it more accurately reflects the distribution of the specific class. (3) When the reasoning prompt is consistent between training and inference, the performance is better than when they are inconsistent. This is expected, as consistency between training and inference ensures that the model can better align the reasoning process across both phases, leading to more coherent and stable results. (4) The inferior performance of the mixed prompt is due to the introduction of information conflict and inconsistency. When using two different prompts, the model needs to balance both, which could lead to confusion in the generated content. Compared to a single prompt, the mixed prompt increases the complexity of reasoning, and the model may not have sufficient capacity to effectively integrate the information from both prompts, thus affecting performance.

4.2.2 Different Number of Prompt Tokens

We conduct an ablation study on the length of the intermediate reasoning prompt, using the universal reasoning prompt as the intermediate reasoning prompt, which samples a set of indices from the image tokenizer’s codebook based on a uniform distribution. To save computational resources, all experiments train the model with 111M parameters for 50 epochs, as 50 epochs are sufficient to reflect the performance of different models. The results are shown in Fig. 4. A prompt length of 0 corresponds to the base-

line, which represent the baseline without intermediate reasoning prompt. We can observe that when the reasoning prompt is short (8 tokens), ability of IGTR to handle complex image generation task is weaker due to containing less information, resulting in performance similar to the baseline. Furthermore, as the length of the prompt increases, the FID performance improves gradually. However, the performance gains are not uncapped, which could be found that when the prompt length reaches near 256 the gains begin to slow down. This phenomenon is reasonable as the gains from using distributed information will reach an upper limit. Therefore, in subsequent experiments, considering both performance and efficiency, the length of reasoning prompt is set to 256.

4.2.3 Order of Reasoning and Generation

A potential benefit of IGTR is that it allows the model to better access relevant knowledge acquired during the pre-training process. To investigate this, we test an alternative configuration where the intermediate reasoning prompt is given only after the image generation, isolating whether the model actually depends on the prior reasoning prompt to generate the image. The experiments train the model for 50 epochs. As shown in the ‘Reasoning After Generation’ row in Table 3, we find that the performance of this variant is comparable to the baseline, suggesting that the sequential reasoning itself is valuable in the generation process of the model, rather than merely activating known knowledge.

4.2.4 Blank Prompt

Another way to think about our IGTR is that the proposed image-related reasoning prompt enables the model to spend more computational resources (*i.e.*, intermediate tokens). To isolate the impact of variable computation from the reasoning process itself, we conduct a variant where we replace the intermediate reasoning prompt with multiple blank tokens of equal length, which are tokens extracted from a completely black image with no distributional information. The experiments train the model for 50 epochs. The experimental result, as shown in ‘Blank Prompt’ of Table 3, indicates that this variant performs similarly to the baseline without our reasoning prompt. This demonstrate that variable computation itself is not the reason for the success

Type	Model	Param	FID↓	IS↑	Precision↑	Recall↑
GAN	BigGAN [2]	112M	6.95	224.5	0.89	0.38
	GigaGAN [13]	569M	3.45	225.5	0.84	0.61
	StyleGAN-XL [30]	166M	2.30	265.1	0.78	0.53
Diffusion	ADM [6]	554M	10.94	101.0	0.69	0.63
	CDM [12]	-	4.88	158.7	-	-
	LDM-4 [27]	400M	3.60	247.7	-	-
	DiT-XL/2 [24]	675M	2.27	278.2	0.83	0.57
Masked AR	MaskGIT [4]	227M	6.18	182.1	0.80	0.51
	MaskGIT-re [18]	227M	4.02	355.6	-	-
	MAGE [19]	230M	6.93	195.8	-	-
AR	VQGAN [8]	227M	18.65	80.4	0.78	0.26
	VQGAN [8]	1.4B	15.76	74.3	-	-
	VQGAN-re [42]	1.4B	5.20	280.3	-	-
	ViT-VQGAN [42]	1.7B	4.17	175.1	-	-
	ViT-VQGAN-re [42]	1.7B	3.04	227.4	-	-
	RQTran. [17]	3.8B	7.55	80.4	0.78	0.26
	RQTran.-re [17]	3.8B	3.80	323.7	-	-
	LlamaGen-B (CFG=2.00) [35]	111M	5.46	193.61	0.83	0.45
	LlamaGen-L (CFG=1.75) [35]	343M	3.81	248.28	0.83	0.52
	LlamaGen-XL (CFG=1.75) [35]	775M	3.39	227.08	0.81	0.54
	LlamaGen-XXL (CFG=1.75) [35]	1.4B	3.09	253.61	0.83	0.53
	IGTR-B (CFG=1.75)	111M	4.39	222.80	0.85	0.46
	IGTR-L (CFG=1.75)	343M	3.23	279.07	0.84	0.52
	IGTR-XL (CFG=1.75)	775M	2.85	289.75	0.83	0.54
	IGTR-XXL (CFG=1.75)	1.4B	2.76	275.80	0.82	0.55

Table 5. Model comparisons on class-conditional ImageNet 256×256 benchmark. Metrics include Frechet inception distance (FID), inception score (IS), precision and recall. ‘-re’ means rejection sampling. ‘↓’ or ‘↑’ indicate lower or higher values are better. ‘CFG’ means using Classifier-Free Guidance.



Figure 5. Sample images randomly generated by IGTR, trained on ImageNet.

of IGTR, and that IGTR expresses intermediate reasoning steps with distributional information to be effective.

4.2.5 Effect of Classifier-Free Guidance (CFG)

We conduct ablation experiments under different Classifier-Free Guidance (CFG) settings based on random reason-

ing prompt, as shown in Table 4. It can be observed that as CFG increases, the model’s performance gradually improves, with the best FID achieved when CFG is set to 1.75. However, further increasing CFG leads to a deterioration in FID. Additionally, the increase in CFG results in a trade-off between diversity and fidelity, with higher accuracy and lower recall. Therefore, in subsequent experiments, we set

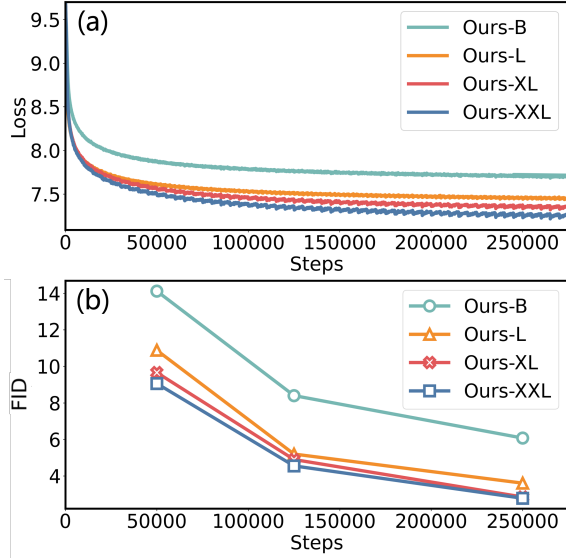


Figure 6. Scaling behavior of IGTR. (a) Training loss of models with different sizes. (b) FID scores of models with different sizes during inference.



Figure 7. Visualization of samples generated by IGTR based on different model sizes.

the CFG to 1.75.

4.3. Main Results

Comparisons with Other Image Generation Methods

In Table 5, we compare with popular image generation models, including GAN [2, 13, 30], Diffusion models [6, 12, 24, 27], masked AR [4, 18, 19] and AR models [8, 17, 35, 42]. All our experiments are based on the universal reasoning prompt, as it is more general and easier to obtain compared to the class reasoning prompt.

The results show that our models outperform all previous AR methods at different levels of model parameters. For example, compared to Llama-B, Llama-L Llama-XL

and Llama-XL with the same parameters, IGTR-B, IGTR-L IGTR-XL and IGTR-XL improves FID by 20%, 15%, 16% and 11%, and IS by 15%, 12%, 28% and 9%, respectively. This indicates that our IGTR of introducing reasoning prompts effectively helps the AR model in learning and generation by enhancing contextual reasoning of generation and improving stability during the generation process through increased inference steps. It is important to note that since LlamaGen does not release the results at 300 epoches for the L and XL models, for a fair comparison, we only present the results for our method at 50 epoches on the XL and XXL models, which have not yet reached the performance limit of our method, leaving room for further improvement.

Visualization As shown in Fig. 5, we visualize some sample images randomly generated by IGTR, trained on ImageNet. This demonstrates that IGTR is capable of generating high-quality samples with both high fidelity and diversity. More visualizations are provided in the appendix.

Scaling Behavior We investigate the scaling behavior of IGTR. As shown in Fig. 6, we show the training loss and FID score based on models of different sizes. It can be observed that IGTR demonstrates good scalability, with lower training loss and better FID scores as the model size increases. This is because we did not modify the formula or structure of the AR model itself, preserving the integrity of the AR framework, and therefore inheriting the scalability of AR methods. Additionally, we visualize the generation results of the same class under different model sizes, as shown in Fig. 7. It can be observed that as the model size increases, the generated results for the same class become more realistic and detailed, with finer textures and better overall consistency.

5. Conclusion

In this work, inspired by the CoT reasoning technique from NLP of AR model, we propose Image Generation with Thoughtful Reasoning (IGTR), to enhance AR image generation. IGTR improves both the accuracy and stability of image generation without changing the model structure or the autoregressive generation order. By adding specialized image-related reasoning prompts, IGTR enhance contextual reasoning by allowing the model to first perceive overall distribution information before generating the image, and improve generation stability by increasing the inference steps. IGTR shows an approximately 20% improvement over the AR baseline, demonstrating the effectiveness of reasoning prompts in complex image generation tasks.

References

- [1] Josh Achiam, Steven Adler, Sandhini Agarwal, Lama Ahmad, Ilge Akkaya, Florencia Leoni Aleman, Diogo Almeida, Janko Altmerschmidt, Sam Altman, Shyamal Anadkat, et al. Gpt-4 technical report. *arXiv preprint arXiv:2303.08774*, 2023. 1
- [2] Andrew Brock. Large scale gan training for high fidelity natural image synthesis. *arXiv preprint arXiv:1809.11096*, 2018. 3, 7, 8
- [3] Tom B Brown. Language models are few-shot learners. *arXiv preprint arXiv:2005.14165*, 2020. 2
- [4] Huiwen Chang, Han Zhang, Lu Jiang, Ce Liu, and William T Freeman. Maskgit: Masked generative image transformer. In *Proceedings of the IEEE/CVF Conference on Computer Vision and Pattern Recognition*, pages 11315–11325, 2022. 2, 7, 8
- [5] Karl Cobbe, Vineet Kosaraju, Mohammad Bavarian, Mark Chen, Heewoo Jun, Lukasz Kaiser, Matthias Plappert, Jerry Tworek, Jacob Hilton, Reiichiro Nakano, et al. Training verifiers to solve math word problems. *arXiv preprint arXiv:2110.14168*, 2021. 2
- [6] Prafulla Dhariwal and Alexander Nichol. Diffusion models beat gans on image synthesis. In *Advances in neural information processing systems*, pages 8780–8794, 2021. 3, 7, 8
- [7] Prafulla Dhariwal and Alex Nichol. Diffusion models beat gans on image synthesis, 2021. 5
- [8] Patrick Esser, Robin Rombach, and Bjorn Ommer. Taming transformers for high-resolution image synthesis. In *Proceedings of the IEEE/CVF conference on computer vision and pattern recognition*, pages 12873–12883, 2021. 2, 7, 8
- [9] Guhao Feng, Bohang Zhang, Yuntian Gu, Haotian Ye, Di He, and Liwei Wang. Towards revealing the mystery behind chain of thought: A theoretical perspective, 2023. 3
- [10] Ian Goodfellow, Jean Pouget-Abadie, Mehdi Mirza, Bing Xu, David Warde-Farley, Sherjil Ozair, Aaron Courville, and Yoshua Bengio. Generative adversarial nets. *Advances in neural information processing systems*, 27, 2014. 3
- [11] Martin Heusel, Hubert Ramsauer, Thomas Unterthiner, Bernhard Nessler, and Sepp Hochreiter. Gans trained by a two time-scale update rule converge to a local nash equilibrium, 2018. 5
- [12] Jonathan Ho, Chitwan Saharia, William Chan, David J Fleet, Mohammad Norouzi, and Tim Salimans. Cascaded diffusion models for high fidelity image generation. *Journal of Machine Learning Research*, 23(47):1–33, 2022. 3, 7, 8
- [13] Minguk Kang, Jun-Yan Zhu, Richard Zhang, Jaesik Park, Eli Shechtman, Sylvain Paris, and Taesung Park. Scaling up gans for text-to-image synthesis. In *Proceedings of the IEEE/CVF Conference on Computer Vision and Pattern Recognition*, pages 10124–10134, 2023. 3, 7, 8
- [14] Tero Karras, Samuli Laine, and Timo Aila. A style-based generator architecture for generative adversarial networks. In *Proceedings of the IEEE/CVF conference on computer vision and pattern recognition*, pages 4401–4410, 2019. 3
- [15] Jacob Devlin Ming-Wei Chang Kenton and Lee Kristina Toutanova. Bert: Pre-training of deep bidirectional transformers for language understanding. In *Proceedings of naacL-HLT*, page 2. Minneapolis, Minnesota, 2019. 2
- [16] Diederik P Kingma. Auto-encoding variational bayes. *arXiv preprint arXiv:1312.6114*, 2013. 3
- [17] Doyup Lee, Chiheon Kim, Saehoon Kim, Minsu Cho, and Wook-Shin Han. Autoregressive image generation using residual quantization. In *Proceedings of the IEEE/CVF Conference on Computer Vision and Pattern Recognition*, pages 11523–11532, 2022. 7, 8
- [18] Tianhong Li, Huiwen Chang, Shlok Mishra, Han Zhang, Dina Katabi, and Dilip Krishnan. Mage: Masked generative encoder to unify representation learning and image synthesis. In *Proceedings of the IEEE/CVF Conference on Computer Vision and Pattern Recognition*, pages 2142–2152, 2023. 2, 7, 8
- [19] Tianhong Li, Yonglong Tian, He Li, Mingyang Deng, and Kaiming He. Autoregressive image generation without vector quantization. *arXiv preprint arXiv:2406.11838*, 2024. 2, 7, 8
- [20] Wang Ling, Dani Yogatama, Chris Dyer, and Phil Blunsom. Program induction by rationale generation: Learning to solve and explain algebraic word problems. *arXiv preprint arXiv:1705.04146*, 2017. 2
- [21] Qing Lyu, Shreya Havaldar, Adam Stein, Li Zhang, Delip Rao, Eric Wong, Marianna Apidianaki, and Chris Callison-Burch. Faithful chain-of-thought reasoning. *arXiv preprint arXiv:2301.13379*, 2023. 2
- [22] Debjyoti Mondal, Suraj Modi, Subhadarshi Panda, Rituraj Singh, and Godawari Sudhakar Rao. Kam-cot: Knowledge augmented multimodal chain-of-thoughts reasoning. In *Proceedings of the AAAI Conference on Artificial Intelligence*, pages 18798–18806, 2024. 2
- [23] Yao Mu, Qinglong Zhang, Mengkang Hu, Wenhai Wang, Mingyu Ding, Jun Jin, Bin Wang, Jifeng Dai, Yu Qiao, and Ping Luo. Embodiedgpt: Vision-language pre-training via embodied chain of thought. *Advances in Neural Information Processing Systems*, 36, 2024. 2
- [24] William Peebles and Saining Xie. Scalable diffusion models with transformers. In *Proceedings of the IEEE/CVF International Conference on Computer Vision*, pages 4195–4205, 2023. 1, 3, 7, 8
- [25] A Radford. Improving language understanding by generative pre-training. 2018. 2
- [26] Aditya Ramesh, Mikhail Pavlov, Gabriel Goh, Scott Gray, Chelsea Voss, Alec Radford, Mark Chen, and Ilya Sutskever. Zero-shot text-to-image generation. In *International conference on machine learning*, pages 8821–8831. Pmlr, 2021. 2
- [27] Robin Rombach, Andreas Blattmann, Dominik Lorenz, Patrick Esser, and Björn Ommer. High-resolution image synthesis with latent diffusion models. In *Proceedings of the IEEE/CVF conference on computer vision and pattern recognition*, pages 10684–10695, 2022. 1, 3, 7, 8
- [28] Olga Russakovsky, Jia Deng, Hao Su, Jonathan Krause, Sanjeev Satheesh, Sean Ma, Zhiheng Huang, Andrej Karpathy, Aditya Khosla, Michael Bernstein, Alexander C. Berg, and Li Fei-Fei. ImageNet Large Scale Visual Recognition Challenge. *International Journal of Computer Vision (IJCV)*, 115 (3):211–252, 2015. 5

- [29] Tim Salimans, Ian Goodfellow, Wojciech Zaremba, Vicki Cheung, Alec Radford, and Xi Chen. Improved techniques for training gans, 2016. [5](#)
- [30] Axel Sauer, Katja Schwarz, and Andreas Geiger. Stylegan-xl: Scaling stylegan to large diverse datasets. In *ACM SIGGRAPH 2022 conference proceedings*, pages 1–10, 2022. [3](#), [7](#), [8](#)
- [31] Noam Shazeer. Glu variants improve transformer, 2020. [5](#)
- [32] Jiaming Song, Chenlin Meng, and Stefano Ermon. Denoising diffusion implicit models. *arXiv preprint arXiv:2010.02502*, 2020. [3](#)
- [33] Yang Song and Stefano Ermon. Generative modeling by estimating gradients of the data distribution. In *Advances in neural information processing systems*, 2019. [3](#)
- [34] Jianlin Su, Yu Lu, Shengfeng Pan, Ahmed Murtadha, Bo Wen, and Yunfeng Liu. Roformer: Enhanced transformer with rotary position embedding, 2023. [5](#)
- [35] Peize Sun, Yi Jiang, Shoufa Chen, Shilong Zhang, Bingyue Peng, Ping Luo, and Zehuan Yuan. Autoregressive model beats diffusion: Llama for scalable image generation. *arXiv preprint arXiv:2406.06525*, 2024. [1](#), [3](#), [5](#), [7](#), [8](#)
- [36] Hugo Touvron, Thibaut Lavril, Gautier Izacard, Xavier Martinet, Marie-Anne Lachaux, Timothée Lacroix, Baptiste Rozière, Naman Goyal, Eric Hambro, Faisal Azhar, et al. Llama: Open and efficient foundation language models. *arXiv preprint arXiv:2302.13971*, 2023. [1](#), [3](#), [5](#)
- [37] Aaron Van Den Oord, Oriol Vinyals, et al. Neural discrete representation learning. In *Advances in neural information processing systems*, 2017. [3](#)
- [38] Xuezhi Wang, Jason Wei, Dale Schuurmans, Quoc Le, Ed Chi, Sharan Narang, Aakanksha Chowdhery, and Denny Zhou. Self-consistency improves chain of thought reasoning in language models. *arXiv preprint arXiv:2203.11171*, 2022. [2](#)
- [39] Jason Wei, Xuezhi Wang, Dale Schuurmans, Maarten Bosma, Fei Xia, Ed Chi, Quoc V Le, Denny Zhou, et al. Chain-of-thought prompting elicits reasoning in large language models. *Advances in neural information processing systems*, 35:24824–24837, 2022. [2](#)
- [40] Shunyu Yao, Dian Yu, Jeffrey Zhao, Izhak Shafran, Tom Griffiths, Yuan Cao, and Karthik Narasimhan. Tree of thoughts: Deliberate problem solving with large language models. *Advances in Neural Information Processing Systems*, 36, 2024. [2](#)
- [41] Jiacheng Ye, Shansan Gong, Liheng Chen, Lin Zheng, Jiahui Gao, Han Shi, Chuan Wu, Xin Jiang, Zhenguo Li, Wei Bi, et al. Diffusion of thoughts: Chain-of-thought reasoning in diffusion language models. *arXiv preprint arXiv:2402.07754*, 2024. [2](#)
- [42] Jiahui Yu, Xin Li, Jing Yu Koh, Han Zhang, Ruoming Pang, James Qin, Alexander Ku, Yuanzhong Xu, Jason Baldridge, and Yonghui Wu. Vector-quantized image modeling with improved vqgan. *arXiv preprint arXiv:2110.04627*, 2021. [2](#), [7](#), [8](#)
- [43] Lijun Yu, Yong Cheng, Kihyuk Sohn, José Lezama, Han Zhang, Huiwen Chang, Alexander G Hauptmann, Ming-Hsuan Yang, Yuan Hao, Irfan Essa, et al. Magvit: Masked generative video transformer. In *Proceedings of the IEEE/CVF Conference on Computer Vision and Pattern Recognition*, pages 10459–10469, 2023. [2](#)
- [44] Biao Zhang and Rico Sennrich. Root mean square layer normalization, 2019. [5](#)
- [45] Zhuosheng Zhang, Aston Zhang, Mu Li, Hai Zhao, George Karypis, and Alex Smola. Multimodal chain-of-thought reasoning in language models. *arXiv preprint arXiv:2302.00923*, 2023. [2](#)

Autoregressive Image Generation Guided by Chains of Thought

Supplementary Material

CFG	FID↓	IS↑	Precision↑	Recall↑
1.25	6.36	146.53	0.74	0.61
1.50	3.16	216.92	0.80	0.57
1.75	3.23	279.07	0.84	0.52
2.00	4.45	326.82	0.87	0.48
2.25	6.02	362.51	0.89	0.44
2.50	7.65	388.27	0.90	0.41

Table 1. Ablation study for different CFG settings for IGTR-L.

CFG	FID↓	IS↑	Precision↑	Recall↑
1.25	5.98	154.40	0.73	0.63
1.50	2.94	229.53	0.79	0.58
1.75	2.85	289.75	0.83	0.54
2.00	3.98	335.43	0.86	0.49
2.25	5.32	369.01	0.88	0.46
2.50	6.69	395.05	0.89	0.42

Table 2. Ablation study for different CFG settings for IGTR-XL.

CFG	FID↓	IS↑	Precision↑	Recall↑
1.25	5.99	153.43	0.72	0.63
1.50	3.09	219.53	0.79	0.60
1.75	2.76	275.80	0.82	0.55
2.00	3.53	320.92	0.85	0.51
2.25	4.50	353.05	0.87	0.49
2.50	5.55	378.07	0.88	0.45

Table 3. Ablation study for different CFG settings for IGTR-XXL.

Top-K	FID↓	IS↑	Precision↑	Recall↑
0	4.39	222.80	0.85	0.46
2000	8.15	244.26	0.87	0.34
4000	6.51	245.63	0.87	0.38
6000	5.61	239.90	0.87	0.41
8000	5.08	236.27	0.86	0.41
10000	4.79	231.78	0.86	0.44
12000	4.55	229.23	0.85	0.45
14000	4.42	225.34	0.85	0.45
16000	4.38	222.93	0.85	0.45

Table 4. The effect of Top-K (CFG=1.75).

Model	FID↓	IS↑	Precision↑	Recall↑
IGTR-B	4.32	219.05	0.85	0.46
IGTR-L	3.08	278.99	0.84	0.52
IGTR-XL	2.79	285.81	0.83	0.54
IGTR-XXL	2.71	262.75	0.82	0.55

Table 5. The effect of utilization of rejection sampling strategy (CFG=1.75, top-k=0).

1. The Effect of Evaluation Configurations

As shown in Table 1 Table 2 and Table 3, we provide the results when adjusting the scale of classifier-free guidance with IGTR-L training for 300 epochs, IGTR-XL training for 50 epochs, IGTR-XXL training for 50 epochs. It can be observed that as the CFG value increases, the model’s performance shows a gradual improvement, reaching the optimal FID. However, further raising the CFG causes a decline in FID. Moreover, the increase in CFG introduces a trade-off between diversity and fidelity, with higher accuracy and lower recall. Considering all ablation experiments on different CFG based on different model scales, we ultimately set the CFG to 1.75.

In addition, we show the ablation experiments on different top-k values with the IGTR-B model which has trained for 300 epochs. Table 4 indicates that IGTR exhibits a similar behavior to that of classic AR models.

Furthermore, as shown in Table 5, we test the influence of the rejection sampling strategy with IGTR-B training for 300, IGTR-L training for 300 epochs, IGTR-XL training for 50 epochs, IGTR-XXL training for 50 epochs. Table 5 indicates that the rejection sampling strategy has little improvement to the inference performance.

All mentioned models are implemented with *Universal Reasoning Prompt* with 256 tokens.

2. Visualization on Generated Samples

2.1. Visualization of Good Results

We provide the visualization of sampled good results in Fig. 1.

2.2. Visualization of the Same Class

We provide the visualization of the same class in Fig. 2, Fig. 3, Fig. 4 and Fig. 5.

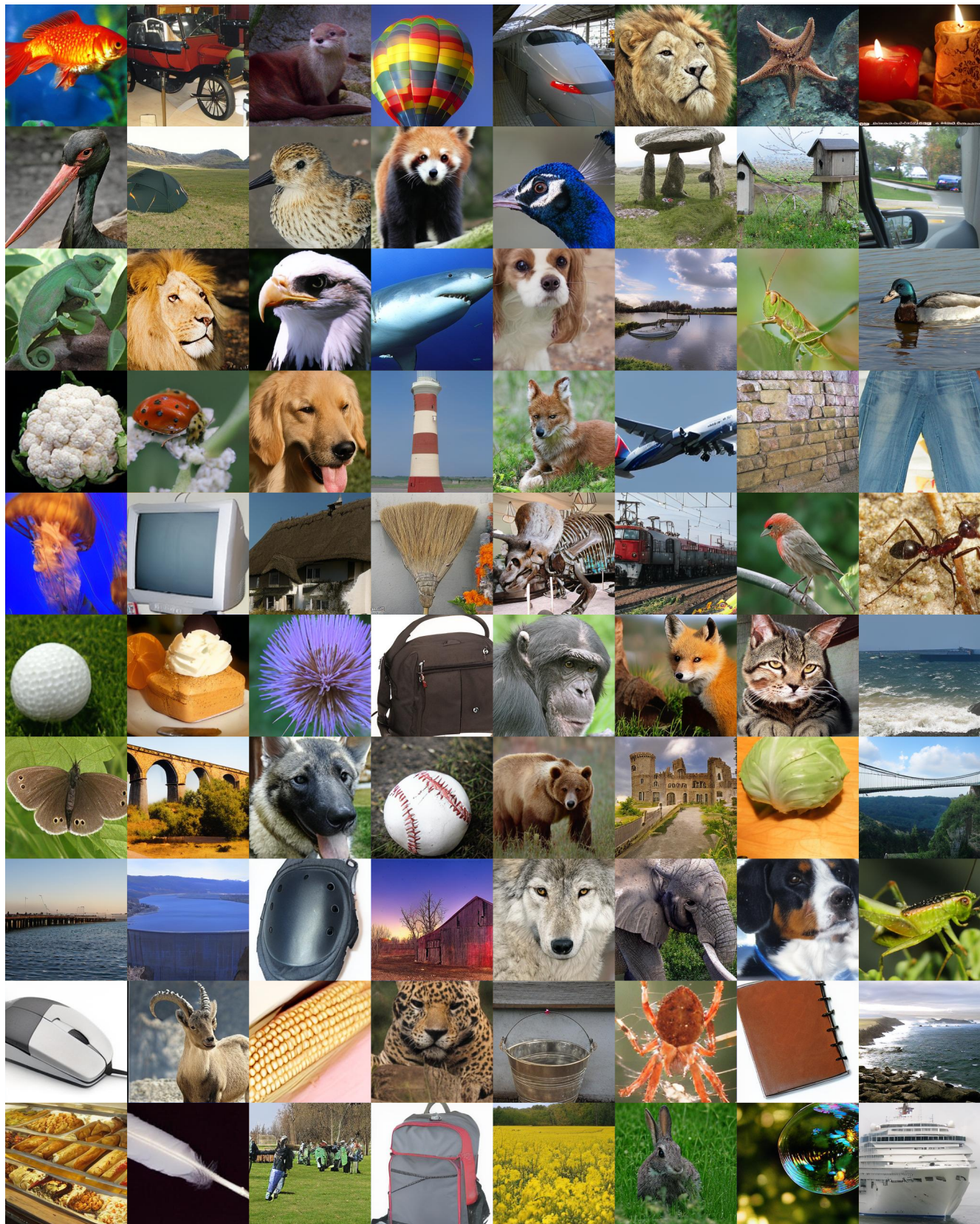


Figure 1. Sample images randomly generated by IGTR, trained on ImageNet.



Figure 2. Visualization results of class 323.



Figure 3. Visualization results of class 970.



Figure 4. Visualization results of class 250.



Figure 5. Visualization results of class 947.



Figure 6. Visualization results of class 358.